Rotational features of vibrator nucleus ^{118}Te

S. Juutinen, A. Savelius, P. T. Greenlees, K. Helariutta, P. Jones, R. Julin, P. Jämsen, H. Kankaanpää, M. Muikku, M. Piiparinen, and S. Törmänen*
Department of Physics, University of Jyväskylä, P.O. Box 35, FIN-40351 Jyväskylä, Finland

M. Matsuzaki
Department of Physics, Fukuoka University of Education, Munakata, Fukuoka 811-4192, Japan
(Received 26 May 1999; published 20 December 1999)

High-spin states in ^{118}Te have been populated via heavy-ion induced reactions. Excited states were observed up to $I=32\hbar$ and, in addition to irregular level sequences, several bands were identified for the first time. The decoupled negative parity bands based upon 7^- and 8^- states are interpreted to arise from the proton $h_{11/2}g_{7/2}$ configuration coupled to the $2p$-$2h$ intruder states in ^{116}Sn. These bands show very smooth alignment behavior, in accordance with the proton $h_{11/2}$ bands in neighboring Sb and I nuclei. Above $I=20$ the yrast positive parity band is built on the proton $h^2_{11/2}$ configuration, also coupled to the proton $2p$-$2h$ excitation. The strongly coupled band built upon the 2914 keV 6^+ state involves a proton hole on the $g_{9/2}$ orbital. Another strongly coupled band based upon the 5006 keV $I=11\hbar$ state was also observed.

PACS number(s): 27.60.+j, 23.20.Lv, 21.10.Re, 25.70.Gh

I. INTRODUCTION

The Te nuclei with 52 protons lie in the transitional region between the spherical nuclei at $Z\approx 50$ and deformed Xe and Ba nuclei. At low spin the Te nuclei are considered to be one of the best examples of quadrupole vibrators. This interpretation stems from the fact that close to twice the energy of the first 2^+ state a multiplet of 0^+, 2^+, and 4^+ states is observed. Furthermore, the energy of the yrast 6^+ state is almost exactly three times the energy of the 2^+ state, as expected in the vibrator picture.

On the other hand, deformed intruder states have been known for a long time in Sn and Sb nuclei. The even-mass Sn nuclei display rotational bands built on excited 0^+ states [1]. These states are believed to arise from proton $2p$-$2h$ excitations, where two $g_{9/2}$ protons are promoted across the $Z=50$ shell gap. Low-lying collective bands in Sb nuclei are explained as related $2p$-$1h$ states [2]. In the simple intruder picture [3] the level pattern of the possible proton $4p$-$2h$ intruder states in ^{118}Te should resemble the one of the $2p$-$4h$ states in ^{114}Cd. In ^{114}Cd and also in other even-mass Cd isotopes near the neutron midshell rather regular band structures at low spin have been observed [4,5]. In Ref. [3] it was suggested that the 958 keV 0^+, 1151 keV 2^+, and 1703 keV 4^+ states form the beginning of the intruder band in ^{118}Te. This pattern is irregular but indeed, the $E0$ and $E2$ transitions from the 958 keV 0^+ state to the ground state and the first 2^+ state are fast, similar to those from the 0^+ band head in ^{114}Cd [4].

Recently, several rotational bands have been found in neutron deficient Sn, Sb, and Te nuclei at high spins [6–17]. They are interpreted to arise from the coupling of deformation driving $h_{11/2}$ protons to the proton $2p$-$2h$ excitations across the $Z=50$ shell gap. Many of these bands display a gradually decreasing moment of inertia, so-called smooth band termination.

The objective of the present investigation was to search for rotational structures in the neutron midshell nucleus ^{118}Te. Deformed states in Sn nuclei minimize their energy around $N=66$ and the same behavior is expected in Te nuclei. Therefore, ^{118}Te is expected to be an ideal nucleus to search for such level structures. The observation of rotational bands in the $Z-1$ neighbor ^{117}Sb also suggests that deformed states might be found in ^{118}Te. However, two short $E2$ cascades reported in Refs. [18,19] were the only candidates for rotational bands in ^{118}Te prior to this work. In the present work, a rich level structure with coexisting noncollective and collective states was observed in ^{118}Te.

II. EXPERIMENTAL METHODS AND RESULTS

In order to investigate excited states in ^{118}Te, two experiments were performed using beams delivered by the $K=130$ MeV cyclotron at the Accelerator Laboratory of the University of Jyväskylä. In the first experiment, the ^{104}Ru(^{18}O,$4n$)^{118}Te reaction was used at a bombarding energy of 65 MeV. The beam was incident upon a 0.6 mg/cm^2 thick gold-backed target. The γ rays were detected by the DORIS array. The second experiment used the ^{100}Mo(^{22}Ne,$4n$)^{118}Te reaction at a bombarding energy of 80 MeV. In this case, the target was a self-supporting 0.6 mg/cm^2 thick foil of ^{100}Mo. The γ rays were detected by the TESSA3 array. The Ge arrays used consist of 12 Tessa-type [20] Compton suppressed Ge detectors. A total of 590 and 80 million γ-γ coincidence events were recorded in the experiments with ^{18}O and ^{22}Ne beams, respectively. In both experiments, the nucleus of interest was the dominant reaction product.

Construction of the level scheme was performed by using the ESCL8R analysis package [21]. The data from the backed-target run was used in order to deduce information concern-

*Present address: The Niels Bohr Institute, Tandem Accelerator Laboratory, DK-4000 Roskilde, Denmark.

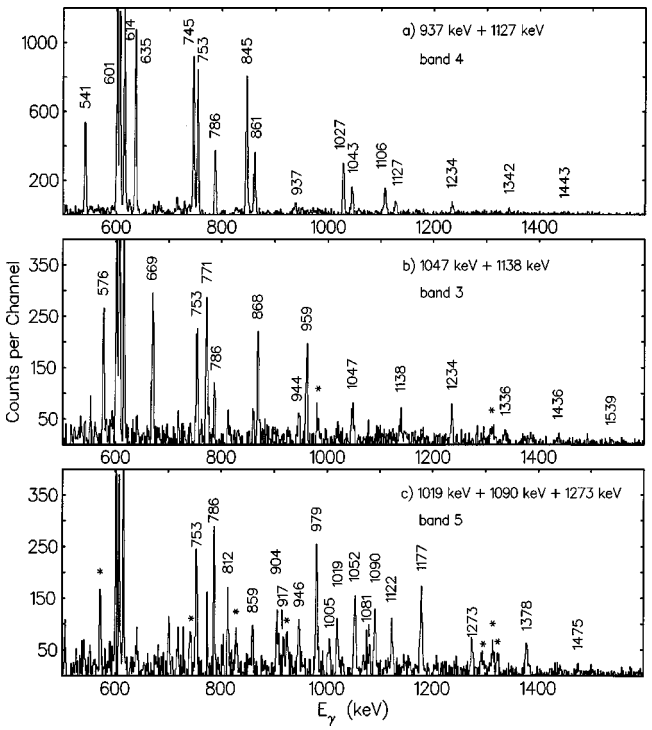

FIG. 1. Examples of γ-ray coincidence spectra for ^{118}Te from the thin-target ^{100}Mo(^{22}Ne,4n) reaction at a bombarding energy of 80 MeV. Peaks marked with an asterisk are due to contaminants.

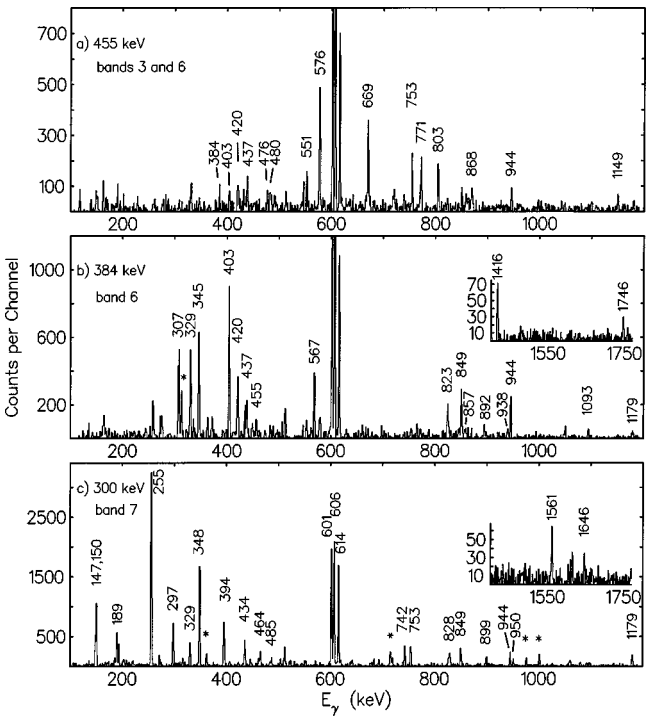

FIG. 2. As in Fig. 1 but for the backed-target ^{104}Ru(^{18}O,4n)^{118}Te reaction at a bombarding energy of 65 MeV.

ing the transition multipolarities. The DORIS frame, of truncated dodecahedron shape, has detectors in four rings at 37°, 78°, 102°, and 143°. To determine the angular distribution ratios the data were sorted into two matrices with the following angle combinations: (i) (37° or 143°) $\times$ all angles and (ii) (78° or 102°) $\times$ all angles, where first the x axis and then the y axis is given. By setting identical y gates on desired γ rays in both matrices coincidence spectra were created which were then used to obtain the intensity ratio $R(E_\gamma)=I_\gamma(E_\gamma;$ extreme angles$)/I_\gamma(E_\gamma;\approx 90°)$. This ratio is about 1.5 for stretched quadrupole and pure $\Delta I=0$ dipole transitions and about 0.8 for pure stretched dipole transitions. However, such R ratios are possible for transitions of mixed multipolarity. In the case of $R<0.8$, the transition can firmly be assigned as $\Delta I=1$, mixed $M1/E2$ type.

A search for isomeric states was made using the centroid-shift method of Ref. [22] and the coincidence data from the backed-target ^{104}Ru(^{18}O,4n) experiment. In this analysis, gates were set on various transitions covering most of the observed level structures and time spectra for the 753 keV $8^+\rightarrow 6^+$ transition and the gating transitions themselves were produced. In the present experiments, the Ge times were recorded against the cyclotron rf signal, which provides a good reference for lifetime measurements. As the result of this lifetime analysis, one isomeric state was identified in ^{118}Te.

Examples of γ-ray coincidence spectra assigned to ^{118}Te and the present level scheme are shown in Figs. 1–3. The energies and intensities of γ rays are listed in Table I. The observed intensities of γ rays in the two reactions were very similar, except for the three rotational bands extending to high spins. In these bands the states above $I\approx 20$ were seen only in the thin-target experiment.

The present level scheme confirms most of the details in the previous level schemes [18,19], but also adds many new transitions between previously known levels and several new level structures. Bands 2 and 4 were earlier reported up to the 13^+ and 19^- states, respectively. From our data two new transitions were added on top of band 2, whereas band 4 [see Fig. 1(a)] was extended by 5 transitions, which are assumed to be of $E2$ type. A new rotational band, band 1, feeding the positive parity yrast and nonyrast $I=2-10$ states, has been established up to the 5721 keV (14^+) level. The spin and parity assignments for the 2517 keV band head are mainly based on the stretched $E2$ character of the 815 and 1311 keV transitions which deexcite to 4^+ states.

Band 3 is identified for the first time in the present experiments. The bottom part of the band is shown in Fig. 2(a). A summed spectrum gated on the higher-lying 1047 and 1138 keV transitions is displayed in Fig. 1(b), depicting the transitions assigned to this band. Band 3 is connected by pure stretched dipole transitions to band 2 and with mixed $M1/E2$ dipole transitions to band 4, therefore this band is assigned negative parity.

Band 5 has been established up to the 16^+ member in previous investigations. From our thin target data several new transitions were added on top of the band, as shown in Fig. 1(c). In the $I^\pi=20^+$ region intensity is distributed between several parallel paths. Band 5 is observed in the present work up to the 15513 keV (32^+) state.

In band 6 only the band head state with a tentative 6^+ spin assignment is reported in the literature [23]. The angular distribution ratios for the depopulating transitions confirm

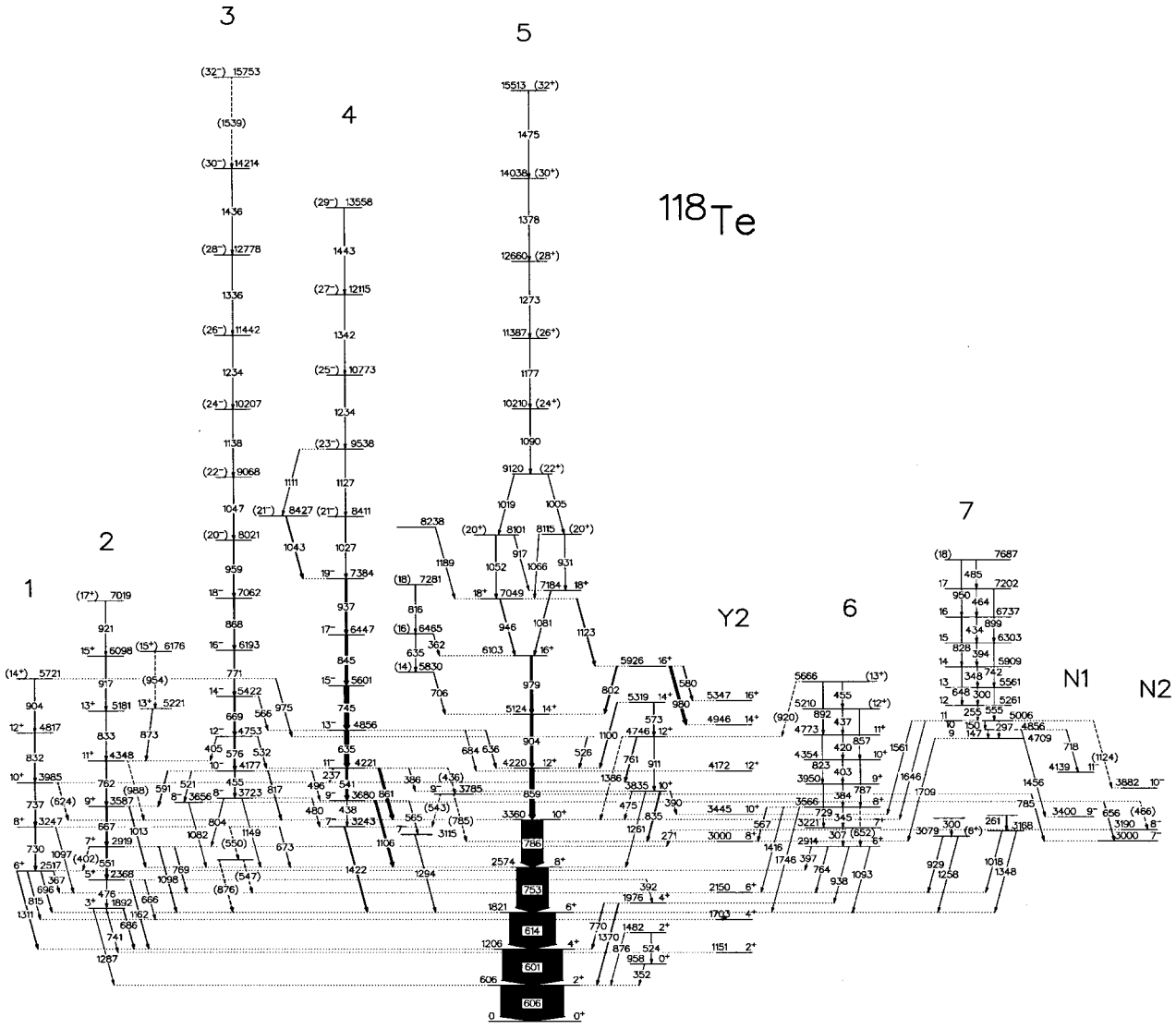

FIG. 3. The level scheme of ^{118}Te deduced in this work.

this spin assignment. The coincidence data allow the band to be built on top of the 6^+ state [see Fig. 2(b)] up to the 5666 keV level with a tentative 13^+ spin assignment. This band has two signatures interconnected by intense dipole transitions. Band 7, also observed for the first time in this work, consists of intense dipole transitions. In this band depopulating transitions are very weak and they carry only a part ($<$50%) of the intensity flowing down from the band. The state at 5006 keV is most likely to be the band head, as the 150 keV transition is of too low energy to belong to the band. A spectrum gated on the 300 keV transition of band 7 is shown in Fig. 2(c).

The rest of the level scheme (cascades $Y1$, $Y2$, $N1$, and $N2$) displays rather irregular level structures and is mostly of noncollective nature. It should be noted that the state at 5926 keV is now deduced to have positive parity, based upon the R ratio for the deexciting transitions. In Ref. [19] the strongly populated 6743 keV state was assigned $I^\pi = 18^-$. A new 1396 keV transition was observed between this state and the yrast 16^+ state at 5347 keV, indicating an $M2$ character for this transition. This does not necessarily contradict the spin/parity assignment, since the Weisskopf estimate for a 1396 keV $M2$ transition is about 0.2 ns, yielding a half-life of approximately 10 ps. The $(6759+\Delta)$ keV level is adopted from Ref. [19]. According to the coincidence relations, this level could be the same as the 6759 keV level previously assigned with spin and parity 18^+. This spin assignment is ambiguous since the angular distribution ratio of 1.9(2) measured for the 1413 keV transition is not consistent with $E2$ character.

The large intensity of the 872 and 603 keV transitions in band $Y1$ indicates that these transitions are yrast and thus support the existence of the $(6759+\Delta)$ keV level and the $I = 19$ assignment for it. The lack of interband transitions between the higher lying states of band $Y1$ and the members of bands 3–5 and $Y2$ may also support this assignment. Parallel to the previously known 872, 603, 808, and 508 keV sequence, other γ-decay paths were identified, and on top of this level structure a few new states were added. Although the parity is unknown in band $Y1$, the measured angular

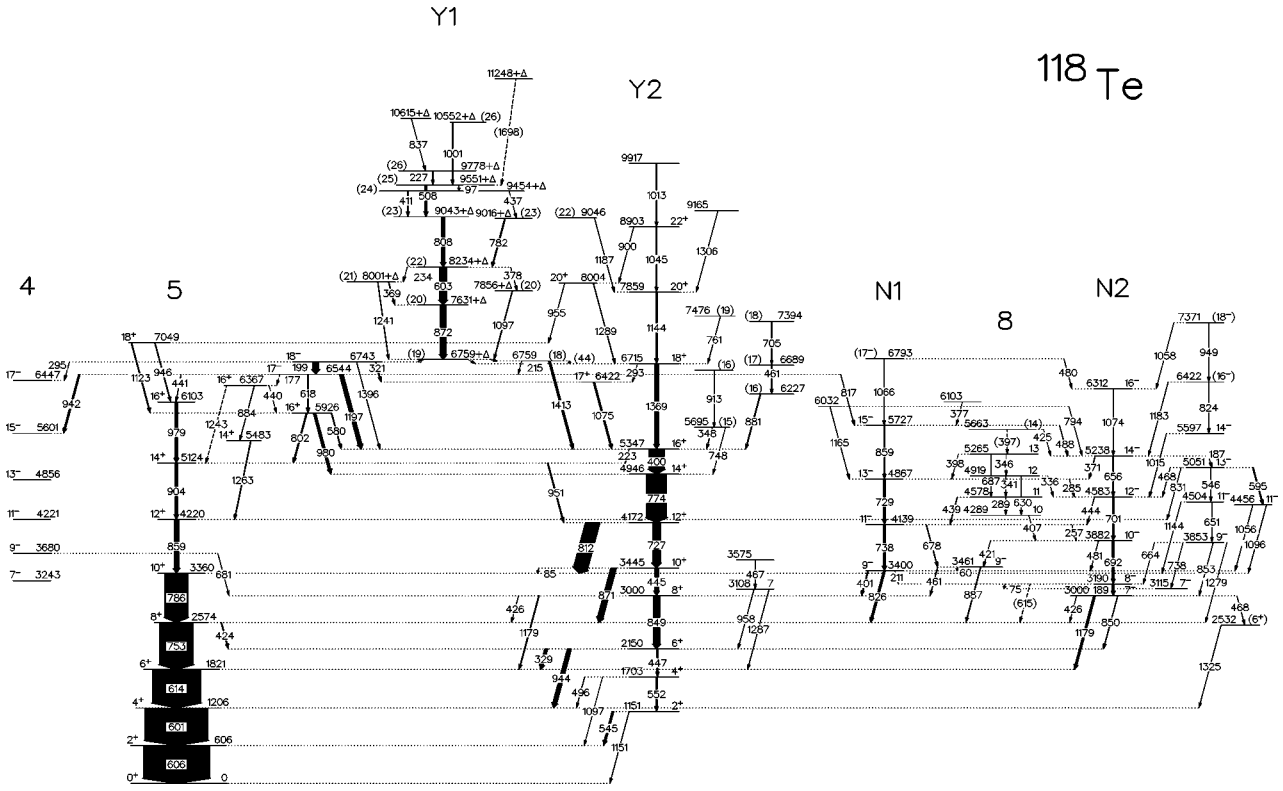

FIG. 3. (*Continued.*)

distribution ratios and the observed combination of dipole and stretched quadrupole transitions imply that the energy levels in band $Y1$ up to the one at $(9016+\Delta)$ keV are of the same parity. The decay from the assumed $(6759+\Delta)$ keV state to the 6715, 6743, and 6759 keV $I=18$ states proceeds by unobserved, very low energy transitions. These branches carry 10, 76, and 14 % of the decay intensity, respectively.

The centroid-shift analysis for this group of transitions revealed that either one of the 6759 and $(6759+\Delta)$ keV levels is isomeric and has a mean lifetime of 1.4(2) ns. If the observed mean lifetime is due to the 6759 keV state, the partial lifetime for the 1413 keV transition is 7(1) ns. This and the measured large angular distribution ratio may indicate that the 1413 keV transition is of mixed $M2/E3$ type. The Weisskopf estimates for the 1413 keV $M2$ and $E3$ transitions are about 0.2 and 180 ns, respectively. On the other hand, a mean lifetime such as measured here could be attributed to a state decaying by low energy $M1$ or $E1$ transitions. The details of the decay from band $Y1$ and the placement of the isomeric state remain to be solved in future experiments.

The $E2$ cascades $N1$ and $N2$ on top of the 3400 keV 9^- and 3190 keV 8^- states have been extended to slightly higher spins than in the earlier work [19]. These bands are now interconnected by many dipole transitions. Between these $E2$ cascades a group of states connected by the 289, 341, 346, and 397 keV transitions is shown, which possibly forms the beginning of a dipole band. The newly observed 5238 keV 14^- state is depopulated by a 187 keV transition to the 5051 keV 13^- state, from which the intensity flows via the 4504 and 4456 keV 11^- states and the 3853 keV 9^- state to the yrast states.

III. DISCUSSION

In all, eight rotational bands and a number of noncollective states were identified in ^{118}Te. Rotational structures corresponding to bands 3–5 in ^{118}Te have been reported in ^{114}Te and ^{116}Te [16,17], but not in the heavier isotopes. A short sequence of $M1$ transitions in ^{120}Te [18] was the only evidence of strongly coupled bands in neighboring Te nuclei prior to this work. The following discussion focuses on the assignment of configurations to the observed level sequences. To facilitate the discussion of the properties of the observed bands, the aligned angular momenta were extracted according to Ref. [24] and are plotted in Fig. 4. The reference used to describe the rotating core is given by the Harris parameters of $J_0=15\hbar^2/\mathrm{MeV}$ and $J_1=25\hbar^4/\mathrm{MeV}^3$ which are adopted from the neighboring Sn and I nuclei [25,26].

In order to investigate the properties of ^{118}Te as a function of spin, potential energy surface (PES) calculations were performed using a code developed by Shimizu [27]. In these calculations it is crucial that the spin is treated as a good quantum number in order to describe the crossing between two bands with largely different shapes. Pairing is introduced by the smoothed gap method with $\Delta=12/\sqrt{A}$ (MeV) for both protons and neutrons. Triaxial deformation is also taken into account. Some of the noncollective minima in PES may not be physical due to calculational reasons. Noncollective states can be constructed in the manner described in Ref. [28]. Calculations were performed for both parities up to spin 31. The present calculations indicate that ^{118}Te is very soft to changes in the deformation. The surfaces for $I^\pi=0^+$, 2^+, and 4^+ show a shallow valley centered around $\epsilon_2\approx 0.17$ and

TABLE I. The γ-ray energies, intensities and $R = I_\gamma(37°$ or $143°)/I_\gamma(79°$ or $101°)$ angular distribution ratios for the transitions assigned to ^{118}Te following the ^{104}Ru(^{18}O,4n) and ^{100}Mo(^{22}Ne,4n) reactions. In the thin-target ^{100}Mo(^{22}Ne,4n) experiment intensities are only given for the yrast and high-spin states.

E_γ	I_γ [a]	I_γ [b]	R [c]	E_i (keV)	I_i^π	I_f^π
43.8(1)	1.6(3)			6759	(18)	18^+
60.1(1)	1.2(3)			3461	9^-	9^-
74.7(1)	3.8(2)			3190	8^-	7^-
84.8(2)	1.9(3)			3445	10^+	10^+
97.1(1)	0.40(6)	1.04(9)		9551+Δ	(25)	(24)
147.3(1)	0.9(2)		0.71(4)	4856	10	9
149.8(1)	0.60(14)		0.76(4)	5006	11	10
177.0(1)	0.62(7)		<0.8	6544	17^-	16^+
187.4(1)	1.93(12)		0.81(4)	5238	14^-	13^-
189.4(1)	43.5(11)		0.93(2)	3190	8^-	7^-
199.0(1)	73(2)		0.67(2)	6743	18^-	17^-
210.8(1)	1.12(9)		1.4(2)	3400	9^-	8^-
215.2(1)	1.24(8)			6759	(18)	17^-
223.0(2)	1.8(2)		1.2(2)	5347	16^+	14^+
226.8(1)	2.1(2)	4.2(2)	0.83(5)	9778+Δ	(26)	(25)
234.2(1)	1.15(7)	1.60(12)	<0.5	8234+Δ	(22)	(21)
236.5(1)	0.93(6)			4221	11^-	10^+
255.1(1)	4.4(2)		1.12(3)	5261	12	11
257.2(1)	1.46(9)		0.37(8)	4139	11^-	10^-
261.0(2)	1.0(3)			3429		
270.6(1)	3.4(2)		0.77(4)	3190	8^-	7^+
284.6(1)	3.6(2)		0.49(3)	4867	13^-	12^-
289.0(1)	0.65(6)		0.89(6)	4578	11	10
293.1(1)	0.87(10)			6715	18^+	17^+
295.5(1)	1.7(2)		0.66(4)	6743	18^-	17^-
297.0(4)	0.90(9)		1.52(6)	5006	11	9
300.1(5)	0.6(3)			3379		(6^+)
300.4(1)	3.40(12)		1.23(4)	5561	13	12
306.8(1)	4.9(2)		1.08(5)	3221	7^+	6^+
320.7(1)	11.3(5)	17.8(6)	0.79(3)	6743	18^-	17^+
329.4(1)	64(2)	63(3)	1.38(2)	2150	6^+	6^+
336.1(1)	1.6(3)		1.41(7)	4919	12	12^-
341.1(1)	1.74(9)		0.88(4)	4919	12	11
345.1(1)	1.70(8)		0.98(9)	5212	(12^-)	13^-
345.2(1)	1.72(14)		1.16(5)	3566	8^+	7^+
346.4(1)	1.03(9)		0.98(8)	5265	13	12
347.6(1)	2.80(10)		1.25(5)	5909	14	13
347.9(1)	7.6(3)		0.81(3)	5695	15	16^+
351.7(4)	1.96(12)			958	0^+	2^+
361.9(3)	1.87(14)		1.34(9)	6465	(16)	16^+
367.1(1)	4.3(2)		1.15(7)	2517	6^+	6^+
369.4(1)	8.6(3)	12.4(5)	0.42(4)	8001+Δ	(21)	(20)
370.9(1)	10.7(4)		0.46(2)	5238	14^-	13^-
376.7(1)	2.24(9)		1.0(2)	6103		15^-
378.0(1)	1.52(7)	2.5(3)	1.40(13)	8234+Δ	(22)	(20)
384.1(1)	3.7(2)		1.13(8)	3950	9^+	8^+
386.2(1)	1.21(9)			4221	11^-	10^+
390.1(1)	3.7(3)		1.5(2)	3835	10^+	10^+
391.9(1)	1.12(9)			2368	5^+	4^+
394.2(1)	1.71(13)		1.22(5)	6303	15	14
396.9(2)	1.5(4)			2914	6^+	6^+

TABLE I. (*Continued.*)

E_γ	I_γ [a]	I_γ [b]	R [c]	E_i (keV)	I_i^π	I_f^π
397.3(2)	1.2(3)			5663	(14)	13
398.0(2)	2.2(2)			5265	13	13^-
400.4(1)	184(5)	360(10)	1.44(3)	5347	16^+	14^+
400.8(1)	28.6(8)		0.78(2)	3400	9^-	8^+
401.9(2)	2.0(2)			2919	7^+	6^+
403.2(1)	2.5(3)		1.12(13)	4354	10^+	9^+
405.0(1)	2.2(2)		0.67(4)	4753	12^-	11^+
407.1(1)	3.9(2)		1.46(8)	4289	10	10^-
411.4(4)	7.7(3)	17.6(6)	0.56(2)	$9454+\Delta$	(24)	(23)
419.0(2)	0.87(12)			2951		6^+
419.8(1)	2.5(3)		1.2(2)	4773	11^+	10^+
420.9(2)	1.71(13)		<0.5	3882	10^-	9^-
423.7(2)	15.0(6)		1.32(5)	2574	8^+	6^+
424.6(2)	1.9(3)			5663	(14)	14^-
425.7(3)	2.2(4)			3000	8^+	8^+
426.1(3)	2.0(2)		1.0(2)	3000	7^-	8^-
433.4(1)	0.9(3)			3680	9^-	8^+
434.2(1)	1.31(9)		1.13(11)	6737	16	15
436.0(5)	1.49(12)			4221	11^-	(9^-)
437.3(1)	1.5(3)			5210	(12^+)	11^+
437.4(5)	0.9(3)	2.0(2)	0.93(9)	$9454+\Delta$	(24)	(23)
437.9(2)	1.12(6)		1.2(2)	3680	9^-	7^-
438.8(1)	6.8(3)		1.46(12)	4578	11	11^-
440				6367	16^+	16^+
440.6(1)	4.1(3)		0.74(5)	6544	17^-	16^+
443.7(1)	6.3(3)		0.43(6)	4583	12^-	11^-
445.2(1)	57(2)	79(3)	1.47(6)	3445	10^+	8^+
447.4(1)	16.2(7)	13.7(5)	1.42(6)	2150	6^+	4^+
454.6(2)	2.8(14)	2.9(2)	1.32(7)	4177	10^-	8^-
455.2(2)	0.78(14)			5666	(13^+)	(12^+)
460.5(1)	3.1(3)			3461	9^-	7^-
461.0(1)	13.1(6)		0.76(4)	3461	9^-	8^+
461.4(1)	6.5(4)		0.68(2)	6689	(17)	(16)
464.4(1)	0.87(9)		1.07(12)	7202	17	16
466.2(2)	0.59(5)			3656	8^-	8^-
467.1(2)	1.2(2)			3575		7
468.2(2)	1.1(2)		0.82(8)	5051	13^-	12^-
468.3(2)	0.6(2)			3000	7^-	(6^+)
475.2(3)	2.2(2)		1.8(3)	3835	10^+	10^+
475.9(2)	5.3(3)		1.31(4)	2368	5^+	3^+
480.1(2)	0.65(7)			3723	8^-	7^-
480.4(2)	1.3(3)			6793	(17^-)	16^-
481.1(1)	6.6(3)		0.45(3)	3882	10^-	9^-
485.3(2)	0.47(7)			7687	(18)	(17)
488.3(1)	5.9(3)		0.55(4)	5727	15^-	14^-
496.2(2)	6.4(5)		1.45(7)	1703	4^+	4^+
496.5(1)	3.4(2)	3.6(3)	0.35(3)	4177	10^-	9^-
508.3(1)	16.8(7)	43(2)	1.51(3)	$9551+\Delta$	(25)	(23)
521.0(1)	2.05(13)	2.2(2)	1.43(7)	4177	10^-	8^-
524.4(5)	0.34(12)			1482	2^+	0^+
526.4(1)	3.1(5)		1.01(14)	4746	12^+	12^+
531.8(1)	5.3(3)	7.6(5)	0.34(4)	4753	12^-	11^-
537.7(1)	1.3(2)			3785	(9^-)	8^+
540.6(1)	34.8(12)	48(2)	1.47(3)	4221	11^-	9^-

TABLE I. (*Continued.*)

E_γ	I_γ [a]	I_γ [b]	R [c]	E_i (keV)	I_i^π	I_f^π
542.6(4)	0.37(11)			3785	(9^-)	7^-
545.1(1)	33.3(3)		0.95(2)	1151	2^+	2^+
546.5(1)	3.8(4)		1.43(7)	5051	13^-	11^-
547.3(3)	3.7(11)			2697		6^+
550.3(1)	4.4(3)			3247	8^+	
551.2(1)	19.9(7)		1.40(3)	2919	7^+	5^+
552.0(1)	19.5(12)		1.33(3)	1703	4^+	2^+
555.0(3)	1.06(9)			5561	13	11
565.1(2)	2.83(12)	3.7(2)	1.4(2)	3680	9^-	7^-
566.1(1)	2.5(3)	4.1(3)	0.4(2)	5422	14^-	13^-
566.5(1)	4.0(6)		1.60(14)	3566	8^+	8^+
573.3(1)	8.3(4)		1.4(2)	5319	14^+	12^+
575.9(1)	18.7(7)	28.5(11)	1.56(5)	4753	12^-	10^-
577.3(3)	0.9(2)			3528		
579.6(1)	9.6(5)		1.55(8)	5926	16^+	16^+
590.6(1)	5.6(3)		0.66(6)	4177	10^-	9^+
594.5(1)	7.2(6)		1.50(7)	5051	11^-	9^-
600.7(1)	1000(30)	1000(40)	1.42(2)	1206	4^+	2^+
603.4(2)	63(6)	148(20)	1.56(3)	$8234+\Delta$	(22)	(20)
605.7(1)	1020(30)	1040(40)	1.42(2)	606	2^+	0^+
614.4(1)	770(30)	880(30)	1.47(2)	1821	6^+	4^+
615.0(4)	6.2(2)			3190	8^-	8^+
617.7(2)	21.8(8)	26.6(14)	0.84(8)	6544	17^-	16^+
624.4(1)	3.4(9)			3985	10^+	10^+
630.1(2)	0.96(11)		1.4(2)	4919	12	10
635.1(1)	58(2)	88(3)	1.43(2)	4856	13^-	11^-
635.1(1)	4.1(3)		1.49(11)	6465	(16)	(14)
636.4(1)	6.4(7)	9.2(13)		4856	13^-	12^+
645.9(1)	2.9(2)		1.2(2)	4867	13^-	11^-
647.9(3)	0.93(6)		1.30(12)	5909	14	12
651.4(1)	6.2(5)		1.53(10)	4504	11^-	9^-
652.3(4)	0.21(6)			3566	8^+	6^+
655.6(1)	19.9(5)		1.40(3)	5238	14^-	12^-
655.7(2)	0.7(2)			3656	8^-	7^-
663.5(2)	2.2(3)		1.1(2)	3853	9^-	8^-
666.0(2)	4.4(7)		1.49(12)	2368	5^+	4^+
667.4(1)	23.9(10)		1.37(7)	3587	9^+	7^+
669.2(1)	20.5(8)	30.1(14)	1.45(3)	5422	14^-	12^-
673.0(3)	4.0(3)		1.3(2)	3247	8^+	8^+
678.1(1)	13.4(5)		1.52(11)	4139	11^-	9^-
680.5(2)	3.7(6)		0.81(8)	3680	9^-	8^+
683.7(3)	3.5(3)		0.97(7)	4856	13^-	12^+
685.8(2)	2.5(3)			1892	3^+	4^+
687.5(1)	1.71(12)		1.59(12)	5265	13	11
692.0(1)	47.9(14)		1.48(2)	3882	10^-	8^-
696.3(1)	14.0(8)		1.06(7)	2517	6^+	6^+
700.9(1)	37.6(13)		1.43(3)	4583	12^-	10^-
704.7(2)	2.9(3)		0.6(2)	7394	(18)	(17)
706.4(1)	4.0(3)		1.22(14)	5830	(14)	14^+
716.2(3)	2.5(3)			4177	10^-	9^-
717.0(5)	1.5(6)		0.46(8)	4856	13^-	11^-
718.0(5)	0.43(11)			4856	10	11^-
727.3(1)	108(4)	169(5)	1.48(2)	4172	12^+	10^+
728.5(1)	38.9(11)		1.46(3)	4867	13^-	11^-

TABLE I. (*Continued.*)

E_γ	I_γ [a]	I_γ [b]	R [c]	E_i (keV)	I_i^π	I_f^π
729.3(2)	1.09(9)		1.4(2)	3950	9^+	7^+
730.1(1)	11.5(5)		1.45(6)	3247	8^+	6^+
737.1(1)	12.8(7)		1.59(5)	3985	10^+	8^+
738.0(2)	3.3(4)		1.31(12)	3853	9^-	7^-
738.2(1)	57(2)		1.44(3)	4139	11^-	9^-
741.0(1)	5.5(3)		1.01(5)	1892	3^+	2^+
742.0(2)	1.09(6)		1.30(11)	6303	15	13
745.2(1)	55(2)	98(4)	1.39(3)	5601	15^-	13^-
747.9(1)	5.3(6)			5695	(15)	14^+
753.1(1)	553(14)	710(20)	1.48(3)	2574	8^+	6^+
761.0(1)	4.5(4)		0.70(14)	7476	(19)	18^+
761.0(1)	3.5(2)		1.36(13)	4746	12^+	10^+
761.5(1)	18.0(7)		1.41(7)	4348	11^+	9^+
763.9(1)	4.7(8)		1.43(10)	2914	6^+	6^+
768.8(1)	12.1(10)		0.74(3)	2919	7^+	6^+
769.9(2)	8.4(2)			1976	4^+	4^+
771.1(1)	10.9(6)	24.1(12)	1.32(3)	6193	16^-	14^-
773.9(1)	261(9)	420(20)	1.52(2)	4946	14^+	12^+
781.8(1)	10.1(4)	20.9(8)	0.56(2)	$9016+\Delta$	(23)	(22)
784.8(3)	2.8(7)			3785	(9^-)	7^-
785.2(3)	2.8(7)			3785	(9^-)	8^+
786.1(1)	360(12)	480(20)	1.47(2)	3360	10^+	8^+
787.0(2)	4.3(9)			4354	10^+	8^+
793.9(2)	2.6(2)			6032		16^-
802.3(1)	5.9(3)		1.55(10)	5926	16^+	14^+
803.6(1)	4.9(4)		0.77(8)	3723	8^-	7^+
808.4(2)	30.8(8)	72(3)	0.89(2)	$9043+\Delta$	(23)	(22)
812.2(1)	199(6)	300(9)	1.52(5)	4172	12^+	10^+
814.6(1)	6.8(4)		1.50(10)	2517	6^+	4^+
816.0(2)	1.92(2)		1.34(9)	7281	(18)	(16)
817.0(1)	1.9(3)			4177	10^-	10^+
817.4(1)	3.4(2)		1.4(2)	6544	17^-	15^-
823.0(2)	1.3(3)		1.4(2)	4773	11^+	9^+
824.3(1)	2.4(2)			6422	(16^-)	14^-
826.4(1)	60(2)		0.79(2)	3400	9^-	8^+
828.1(2)	1.02(9)		1.2(2)	6737	16	14
830.6(1)	3.5(2)			5051	13^-	12^+
832.5(1)	9.6(4)		1.42(7)	4817	12^+	10^+
832.9(3)	10.1(6)		1.55(5)	5181	13^+	11^+
835.4(1)	21.2(12)		1.46(6)	3835	10^+	8^+
837.0(1)	1.3(2)	2.8(2)		$10615+\Delta$		(26)
845.5(1)	26.4(10)	55(2)	1.43(3)	6447	17^-	15^-
849.4(1)	123(5)	130(5)	1.40(5)	3000	8^+	6^+
850.1(1)	9.2(6)		0.88(2)	3000	7^-	6^+
852.6(2)	1.8(3)			3853	9^-	7^-
856.7(2)	1.9(4)			5210	(12^+)	10^+
859.3(1)	15.2(2)		1.55(7)	5727	15^-	13^-
859.5(1)	89(3)	99(4)	1.44(3)	4220	12^+	10^+
861.1(1)	34.8(13)	52(2)	0.83(2)	4221	11^-	10^+
868.2(1)	6.6(4)	20.0(8)	1.4(2)	7062	18^-	16^-
871.0(1)	77(3)	120(4)	1.50(10)	3445	10^+	8^+
871.9(2)	74(4)	128(5)	0.70(2)	$7631+\Delta$	(20)	(19)
873.2(1)	6.6(4)		1.28(7)	5221	13^+	11^+
876.2(1)	10.6(9)			2697		6^+

TABLE I. (*Continued.*)

E_γ	I_γ [a]	I_γ [b]	R [c]	E_i (keV)	I_i^π	I_f^π
876.2(3)	1.24(7)			1482	2^+	2^+
880.8(1)	14.6(7)		1.60(6)	6227	(16)	16^+
883.6(1)	1.5(2)			6367	16^+	14^+
886.6(1)	14.9(6)		0.86(12)	3461	9^-	8^+
892.1(2)	0.92(9)			5666	(13^+)	11^+
898.7(2)	0.95(9)		1.4(2)	7202	17	15
899.7(2)	2.9(2)	3.7(4)		8903	22^+	20^+
903.7(1)	34.8(11)	55(2)	1.25(4)	5124	14^+	12^+
904.1(1)	3.5(2)			5721	(14^+)	12^+
911.1(1)	9.3(10)		1.35(7)	4746	12^+	10^+
913.0(2)	1.6(3)		0.5(2)	6608	(16)	(15)
916.9(1)	3.8(2)		1.3(2)	6098	15^+	13^+
917.2(1)	1.06(10)	2.8(4)		8101	(20^+)	18^+
919.8(1)	1.9(2)			5666	(13^+)	12^+
921.0(1)	0.90(7)			7019	(17^+)	15^+
928.6(2)	1.68(14)			3079	(6^+)	6^+
931.5(3)	0.6(3)	4.4(4)		8115	(20^+)	18^+
936.9(1)	9.3(9)	33.2(13)	1.49(5)	7384	19^-	17^-
938.0(4)	1.9(6)		1.2(2)	2914	6^+	4^+
942.3(1)	22.7(10)	32.2(13)	1.61(4)	6544	17^-	15^-
943.8(1)	91(3)	87(3)	1.45(3)	2150	6^+	4^+
946.2(1)	4.9(2)	13.2(8)	1.6(2)	7049	18^+	16^+
948.9(1)	4.0(2)		1.2(2)	7371	(18^-)	16^-
950.4(2)	0.64(9)			7687	(18)	16
951.1(1)	14.3(8)		1.39(14)	5124	14^+	12^+
954.1(1)	2.9(2)			6176	(15^+)	13^+
954.5(2)	3.1(6)			8004	20^+	18^+
957.6(2)	4.0(3)			3108	7	6^+
959.4(1)	3.5(2)	16.5(6)		8021	(20^-)	18^-
975.1(1)	1.5(6)			5721	(14^+)	12^+
979.0(1)	20.2(10)	51(2)	1.33(7)	6103	16^+	14^+
980.1(1)	31.7(12)	53(2)	1.43(3)	5926	16^+	14^+
988.0(4)	2.2(3)			4348	11^+	10^+
1001.2(1)	4.3(3)	13.8(5)	0.25(5)	$10552+\Delta$	(26)	(25)
1004.9(4)	0.6(3)	4.0(4)		9120	(22^+)	(20^+)
1012.8(3)	4.7(7)			3587	9^+	8^+
1013.4(1)	5.4(3)	10.6(6)		9917		22^+
1014.9(1)	10.5(4)		1.55(8)	5597	14^-	12^-
1018.0(5)	2.6(2)			3168		6^+
1018.6(2)	1.34(13)	4.6(2)		9120	(22^+)	(20^+)
1026.9(1)	3.1(6)	19.9(7)		8411	(21^-)	19^-
1043.4(1)	3.5(2)	12.1(6)		8427	(21^-)	19^-
1044.6(1)	5.9(3)	13.5(6)	1.26(5)	8903	22^+	20^+
1047.5(1)	1.9(2)	11.1(5)		9068	(22^-)	20^-
1052.1(2)	1.9(2)	12.4(7)		8101	(20^+)	18^+
1056.1(1)	1.5(3)		1.33(14)	4456	11^-	9^-
1058.1(2)	2.8(2)			7371	(18^-)	(16^-)
1066.0(1)	6.9(3)		1.2(2)	6793	(17^-)	15^-
1066.1(10)	0.9(6)	3.6(8)		8115	(20^+)	18^+
1074.3(1)	10.0(4)		1.30(6)	6312	16^-	14^-
1075.0(1)	27(2)	31.6(11)	0.40(2)	6422	17^+	16^+
1080.7(1)	4.1(2)	9.0(5)	1.5(3)	7184	18^+	16^+
1081.9(3)	1.2(3)		1.4(2)	3656	8^-	8^+
1089.9(2)	0.65(10)	7.6(7)		10210	(24^+)	(22^+)

TABLE I. (*Continued.*)

E_γ	I_γ [a]	I_γ [b]	R [c]	E_i (keV)	I_i^π	I_f^π
1093.4(1)	6.88(11)		1.40(9)	2914	6^+	6^+
1096.2(1)	5.9(10)		0.82(4)	4456	11^-	10^+
1097.0(2)	4.7(6)		1.33(9)	1703	4^+	2^+
1097.0(2)	1.4(2)		1.3(2)	3247	8^+	6^+
1097.3(1)	8.4(3)	11.1(5)	0.40(4)	7856+Δ	(20)	(19)
1098.1(1)	14.6(6)		0.69(3)	2919	7^+	6^+
1099.7(1)	10.6(10)		1.22(10)	5319	14^+	12^+
1106.3(1)	42.0(12)	42(2)	0.79(2)	3680	9^-	8^+
1111.0(2)	0.66(7)	2.0(4)		9538	(23^-)	(21^-)
1122.5(1)	6.3(3)	17.2(9)	1.47(14)	7049	18^+	16^+
1124.0(2)	0.40(7)		0.7(3)	5006	11	10^-
1126.9(1)	1.6(3)	6.5(3)		9538	(23^-)	(21^-)
1138.4(2)		4.3(3)		10207	(24^-)	(22^-)
1143.6(1)	12.0(4)	28.6(11)	1.53(5)	7859	20^+	18^+
1144.1(1)	1.9(4)			4504	11^-	10^+
1148.5(3)	2.9(3)		1.8(4)	3723	8^-	8^+
1150.8(2)	9.6(10)		1.28(5)	1151	2^+	0^+
1161.6(1)	12.1(6)		1.10(4)	2368	5^+	4^+
1165.2(1)	2.50(13)			6032		13^-
1177.2(2)		6.4(8)		11387	(26^+)	(24^+)
1178.8(1)	21.4(12)		1.33(6)	3000	8^+	6^+
1179.3(1)	51(2)		0.81(5)	3000	7^-	6^+
1183.4(3)	3.2(2)		1.3(2)	6422	(16^-)	14^-
1187.0(3)	2.2(2)	4.4(5)	1.4(2)	9046	(22^+)	20^+
1189.0(5)	1.9(3)	4.3(4)		8238		18^+
1197.1(1)	59(2)	82(3)	0.80(1)	6544	17^-	16^+
1234.1(3)		3.7(3)		10773	(25^-)	(23^-)
1234.4(3)		3.6(3)		11442	(26^-)	(24^-)
1241.3(1)	5.9(2)		1.64(9)	8001+Δ	(21)	(19)
1243.2(3)	2.85(13)		1.7(3)	6367	16^+	14^+
1257.9(3)	3.2(3)			3079	(6^+)	6^+
1261.1(1)	2.5(3)			3835	10^+	8^+
1263.6(1)	3.32(14)		1.34(13)	5483	14^+	12^+
1273.2(3)		2.5(5)		12660	(28^+)	(26^+)
1279.3(2)	3.9(5)		0.95(9)	3853	9^-	8^+
1286.6(2)	3.2(4)		0.98(6)	1892	3^+	2^+
1287.1(2)	6.5(7)		0.72(8)	3108	7	6^+
1288.9(2)	3.2(3)	8.1(5)	1.39(12)	8004	20^+	18^+
1294.2(1)	16.8(10)	8.2(9)	0.88(4)	3115	7^-	6^+
1306.0(4)	1.37(13)	2.8(4)		9165		20^+
1311.2(1)	9.9(6)		1.47(8)	2517	6^+	4^+
1325.4(2)	6.2(7)			2532	(6^+)	4^+
1336.0(5)		2.0(4)		12778	(28^-)	(26^-)
1341.7(4)		2.0(4)		12115	(27^-)	(25^-)
1347.6(3)	2.8(2)			3168		6^+
1368.5(1)	39.5(12)	79(3)	1.55(5)	6715	18^+	16^+
1370.5(2)	8.7(2)			1976	4^+	2^+
1378.0(10)		2.0(7)		14038	(30^+)	(28^+)
1385.7(3)	1.6(7)			4746	12^+	10^+
1396.2(2)	3.6(4)	5.4(4)	1.32(13)	6743	18^-	16^+
1412.5(1)	17.0(4)	35.4(14)	1.9(2)	6759	(18)	16^+
1416.0(2)	1.37(11)			3566	8^+	6^+
1421.5(1)	5.7(3)		0.87(11)	3243	7^-	6^+
1436.0(5)		1.2(2)		14214	(30^-)	(28^-)

TABLE I. (*Continued.*)

E_γ	I_γ [a]	I_γ [b]	R [c]	E_i (keV)	I_i^π	I_f^π
1443.0(10)		1.2(2)		13558	(29^-)	(27^-)
1455.9(5)	0.59(7)		0.8(2)	4856	10	9^-
1475.0(10)		0.8(4)		15513	(32^+)	(30^+)
1539.0(10)		0.4(2)		15753	(32^-)	(30^-)
1560.8(4)	0.9(2)		0.98(10)	5006	11	10^+
1597.2(1)	2.6(2)	9.2(4)				
1646.1(4)	0.4(2)		0.8(3)	5006	11	10^+
1698.0(5)	0.3(1)	2.8(3)		$11248+\Delta$		(25)
1709.1(5)	0.5(2)		0.7(3)	4709	9	8^+
1745.7(3)	0.68(12)				8^+	6^+

[a]In ^{104}Ru(^{18}O,4n) reaction at 65 MeV bombarding energy.
[b]In ^{100}Mo(^{22}Ne,4n) reaction at 80 MeV bombarding energy.
[c]For known stretched quadrupole and dipole transitions angular distribution ratios of about 1.4 and 0.8 were obtained.

ranging from $\gamma\approx-60°$ to large positive γ values, see Fig. 5(a) for $I^\pi=2^+$. At higher spins, deeper energy minima in the $\epsilon-\gamma$ plane appear. Some bands were predicted, as shown in Fig. 6, which were identified with experimentally observed ones, and some others whose correspondence to the data is not clear.

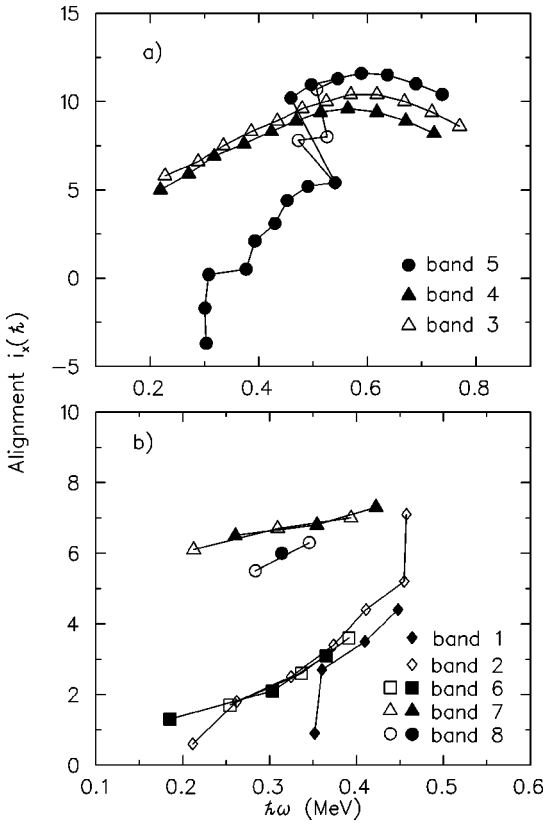

FIG. 4. Aligned angular momenta of bands in ^{118}Te. A reference spin calculated using Harris parameters of $J_0=15\,\hbar^2$/MeV and $J_1=25\,\hbar^4$/MeV^3 has been subtracted. In band 5 two decay paths are included in the $I\approx20\hbar$ region.

A. Decoupled positive-parity bands

1. Band 5

A characteristic of band 5 at low spins is that the level spacing between the two consecutive levels is nearly constant, a feature which is indicative of vibrational behavior. However, above the 6^+ state the vibrational pattern breaks down and the transition energies start to increase with spin which is typical for a rotational band. Finally, above spin 20, a well deformed rotational band develops. The aligned angular momentum in Fig. 4(a) shows gains at frequencies of 0.30, $\approx$0.45, and 0.50 MeV, reaching a value of about $12\hbar$ at $\hbar\omega=0.6$ MeV, which is as large as in the more stably deformed isotone ^{120}Xe [29].

The PES calculations predict two different even spin, positive parity bands which are most likely to be related with band 5. First, in the $I=6-20$ region a strongly triaxial ($\epsilon_2=0.17$, $\gamma\approx-25°$) band develops. Note that Ref. [28] predicts a weakly deformed prolate shape at low spins. The $B(E2)$ values of 81(27) and 94(11) W.u. for the yrast $8^+\rightarrow6^+$ and $10^+\rightarrow8^+$ transitions, respectively, from a recent lifetime measurement [30] are quite consistent with the predicted shape. The shape of ^{118}Te from our PES calculation is very favorable for an $h_{11/2}$ neutron alignment, and the calculations suggest a gradual alignment of a neutron pair around spin 12–14. Secondly, a well deformed band with $\epsilon_2=0.29$, $\gamma\approx+13°$ is predicted. This band is calculated to cross the less deformed triaxial band at spin 18, as shown in Fig. 6(a). What drives the nucleus to such a large deformation is that the configuration of the well-deformed band involves an intruder proton $2p$-$2h$ excitation coupled to two protons on the $h_{11/2}$ orbital. The same configuration has been assigned to the yrast band in ^{116}Te [17]. The calculated deformation for ^{118}Te may sound large, but it is close to the deformation extracted for the $\pi h_{11/2}\otimes2p$-$2h$ configuration in ^{113}Sb [10]. Although the calculated energies are somewhat lower than the experimental ones, the two bands from the PES reproduce the general behavior of band 5 very well. Since the shapes of the two bands are largely different, a

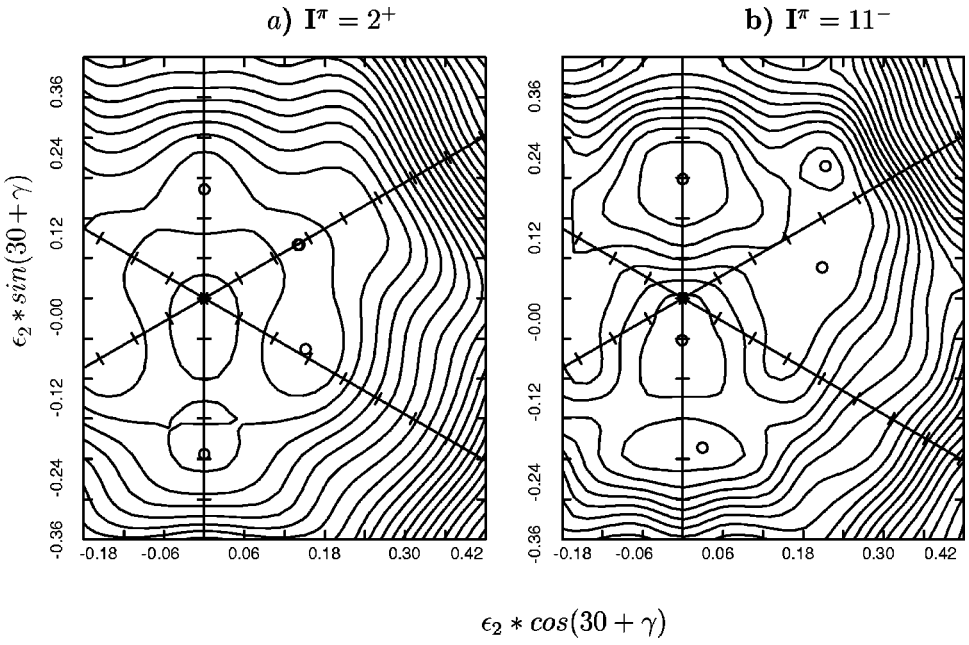

FIG. 5. Potential energy surfaces for (a) $I^\pi = 2^+$, (b) $I^\pi = 11^-$ in ^{118}Te. Energy minima are marked by a circle.

standard cranking calculation with the shape of the low-spin side cannot reproduce this crossing.

2. Bands 1 and 2

Two other decoupled bands, bands 1 and 2, are assigned as having positive parity. Starting from the 8^+ state, both of these bands show a gradual increase in the alignment [see Fig. 4(b)] and the energy splitting between them is small. In the neighboring even-mass Te nuclei [18,19], no bands corresponding to bands 1 and 2 in ^{118}Te have been found.

Different scenarios were considered to explain bands 1 and 2. In particular, band 2 starts at very low excitation energy and in a previous study it has been interpreted as the odd-spin sequence of the γ band [18]. However, the even-spin sequence is usually energetically favored at low spin, as in ^{120}Xe [29]. This is not the case for bands 1 and 2 in ^{118}Te. Note also that in the vibrator picture the 3^+ state at the bottom of band 2 is a member of three-quadrupole phonon multiplet.

In the PES calculation we obtained an odd-spin sequence which corresponds to band 2 in ^{118}Te very well, but no band corresponding to band 1. Since γ vibration is not included in the PES calculation, this indicates that band 2 is a two-quasiparticle excitation on top of band 5, rather than the odd-spin sequence of the γ band. The calculated shape is very similar to that of the triaxial band reproducing band 5 at intermediate spin values. The value of γ deformation shifts considerably with increasing spin, evolving from $-45°$ at $I=3$ to $-14°$ at $I=15$. The present PES calculation gives only the lowest energy states of each parity, signature, and shape. Thus the result that the present calculation does not give a band which corresponds to the observed band 1, hints that band 1 is another two-quasiparticle band with the same shape.

As the nuclear shape calculated for band 2 is optimal for the $h_{11/2}$ neutrons, this band may be built on a less aligned

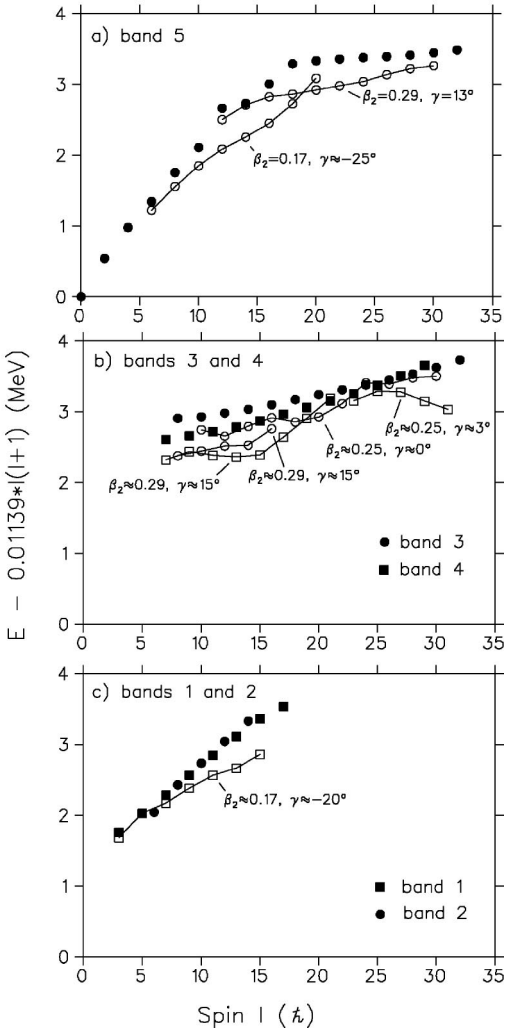

FIG. 6. Rigid rotor plots showing comparison of experimental (filled symbols) and calculated (open symbols) values for bands 1–5 in ^{118}Te.

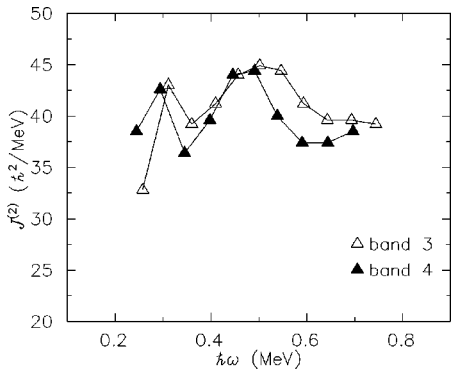

FIG. 7. Dynamic moment of inertia for bands 3 and 4 in ^{118}Te.

$h_{11/2}^2$ configuration. In the CSM picture with *E*, *F*, *G*, and *H* labels for the lowest negative parity states, this involves the first (*E*) and third (*G*) $h_{11/2}$ orbital giving a band with $\alpha=1$, i.e., an odd-spin sequence. According to CSM calculations at the predicted shape, the *EG* configuration is expected at about 500 keV above the *EF* configuration, in reasonable agreement with the position of band 2 relative to band 5 at $\hbar\omega=0.40$ MeV. The $\alpha=0$ *EH* and *F*G configurations lie too high in excitation energy to reproduce the small energy splitting between bands 1 and 2.

Another possibility to explain bands 1 and 2 involves the $g_{7/2}$ and $d_{5/2}$ protons coupled to the intruder band in ^{116}Sn. This may not be completely unrealistic, since in the isotone ^{117}Sb related bands with a single $g_{7/2}$ or $d_{5/2}$ protons have been found [13]. In this scenario, the even-spin sequence should be favored in energy. One more possible interpretation is presented in Sec. III D.

B. Decoupled negative parity bands

In Ref. [19] a portion of band 4 of Fig. 3 was observed and assigned as the $\pi h_{11/2}g_{7/2}$ configuration. Band 3 identified in this work shows a level pattern very similar to that of band 4. Furthermore, the lower portions of the bands are connected by intraband $\Delta I=1$ transitions. Therefore, bands 3 and 4 appear to be signature partners. Inspired by the interpretation of the rotational bands in ^{117}Sb [13,14], we interpret bands 3 and 4 to arise from the coupling of the proton $h_{11/2}g_{7/2}$ configuration to the intruder band in ^{116}Sn.

The alignment plots shown in Fig. 4(a) demonstrate that the aligned angular momentum increases very smoothly in bands 3 and 4, with no sudden alignment gain. According to cranked-shell model (CSM) calculations at a deformation of $\beta_2\approx0.25$, the first quasiparticle alignment in Te nuclei is expected to be due to the $h_{11/2}$ neutrons and to occur at $\hbar\omega\approx0.35$ MeV. In order to reveal smooth band crossings, the dynamic moment of inertia, $J^{(2)}$, is displayed in Fig. 7 for bands 3 and 4. The moment of inertia plots indicate that lowest members of both bands are slightly displaced in energy, possibly due to mixing with other close-lying states. Furthermore, an bump indicating the occurrence of band crossing is observed in both bands close to $\hbar\omega=0.50$ MeV, which is a considerably higher crossing frequency than that predicted by the CSM calculations.

The PES calculations predict [see Fig. 5(b)] well-deformed negative-parity rotational bands, in agreement with the assignment given above. Two minima are predicted. The minimum around $\epsilon_2=0.29$ and $\gamma\approx+15°$ is lowest near the band heads, whereas the other minimum with somewhat lower quadrupole deformation and less positive γ deformation becomes lowest at higher spins. However, the calculated energies stagger and they do not give a very good description of the observed bands.

Rotational bands have now been observed in all $N=66$ isotones from ^{116}Sn to ^{120}Xe and the development of these bands is of interest. In ^{116}Sn, the intruder band built on the proton $2p$-$2h$ excitations undergoes an $h_{11/2}$ neutron alignment at a rotational frequency of 0.46 MeV [25], with a gain in alignment of $\Delta i_x\approx5\hbar$. Below the neutron alignment, TRS calculations predict a deformation of about $\beta_2=0.25$, whereas the neutron alignment is predicted to polarize the nucleus to a smaller deformation. The odd-mass ^{117}Sb and ^{119}I nuclei display very gradual alignment gains in the proton $h_{11/2}$ bands with smeared and delayed neutron $h_{11/2}$ alignments [13,14,26]. In ^{120}Xe the $\pi h_{11/2}g_{7/2}$ bands [29] show very similar alignment patterns with gradual alignment gains as observed in bands 3 and 4. The gradual increase in aligned angular momentum across the expected neutron $h_{11/2}$ alignment region is thus a common feature for bands involving the deformation driving proton $h_{11/2}$ configuration in $N=66$ nuclei. Well-deformed rotational bands in ^{117}Sb [13,14] and ^{118}Te, and to some extent in heavier isotones, are thought to arise from the coupling of protons to the intruder band in ^{116}Sn, i.e., to involve the excitation of two protons from the up-sloping $g_{9/2}$ orbital to the down-sloping orbitals above the $Z=50$ shell gap.

Another interesting feature in bands 3 and 4 is the development of the signature splitting with increasing rotational frequency. At low frequencies, band 4 with signature $\alpha=1$ is energetically favored by about 300 keV. With increasing rotation the energy splitting decreases and finally above $\hbar\omega=0.65$ MeV band 3 with signature $\alpha=0$ becomes energetically favored. The same, but less pronounced trend is also seen between the corresponding bands in ^{120}Xe [29]. CSM calculations have been performed at $\beta_2\approx0.25$ with varying γ deformation around 0° in order to determine how the energy splitting between the lowest positive parity $\alpha=1/2$ and $-1/2$ signatures originating from the spherical $d_{5/2}$ and $g_{7/2}$ orbitals varies with γ deformation. These two signatures are thought to be involved in bands 3 and 4 and to be responsible for the observed energy splitting. For positive values of γ deformation the CSM calculations predict the $\alpha=-1/2$ signature to be favored over the $\alpha=1/2$ signature, in accordance with experiment at low and intermediate rotational frequencies. The calculations suggest that the $\alpha=1/2$ signature becomes favored for negative values ($\approx-10°$) of γ deformation. Since the pair of aligned $h_{11/2}$ neutrons is expected to drive the nuclear shape towards a negative γ deformation, the development of the energy splitting between bands 3 and 4 may represent a gradual shift from a small positive γ deformation towards a negative γ deformation. This evolution is different than in lighter Te nuclei [16,17], where a gradual

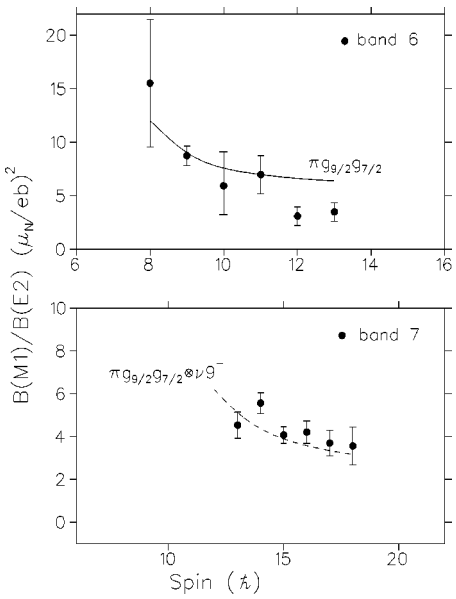

FIG. 8. $B(M1)/B(E2)$ ratios for bands 6 and 7 in ^{118}Te. The experimental values are extracted assuming multipolarity mixing ratio $\delta=0$ for $\Delta I=1$ transitions. In the theoretical estimates (lines) a quadrupole moment of $Q_0=3.0$ *e* b was assumed. The *g* factors for the quasiparticles were adopted from Ref. [33] and g_R was taken as Z/A.

drift towards a deformed noncollective shape, termed as soft band termination, is observed in the proton intruder bands.

C. Strongly coupled bands

Two, possibly three, bands (bands 6–8) with intense dipole transitions have been identified in ^{118}Te. The occurrence of such bands is a common feature in this mass region. Based on observations in the neighboring $N=66$ nuclei, a hole in the proton $g_{9/2}$ orbital is the most likely cause for level sequences of this type. Using the in-band $B(E2,I\rightarrow I-1)/B(E2,I\rightarrow I-2)$ ratios the *K* values were calculated to be 5–6 and 8–9 in bands 6 and 7, respectively. The $E2$ components of the $I\rightarrow I-1$ transitions were estimated from the angular distribution ratios. Band 8 is very weakly populated and no estimate for the *K* value was obtained. The aligned angular momenta extracted for the dipole bands are shown in Fig. 4(b).

To aid the determination of the configurations involved, $B(M1,I\rightarrow I-1)/B(E2,I\rightarrow I-2)$ ratios were also extracted in bands 6 and 7. Such ratios are sensitive to the g_K factors of the quasiparticles and the quadrupole moment of the band. Experimental $B(M1)/B(E2)$ ratios together with theoretical estimates obtained from a geometrical model [31,32] are shown in Fig. 8.

The energy of the lowest state in band 6 implies that this band is built on a two-quasiparticle configuration. We assign the proton $g_{9/2}^{-1}g_{7/2}$ (or $g_{9/2}^{-1}d_{5/2}$) configuration to this band. An initial alignment of about $1.5\hbar$ for band 6 in Fig. 4(b) is due to the quasiparticle occupying the $g_{7/2}$ orbital. The theoretical $B(M1)/B(E2)$ ratios calculated for the $g_{9/2}^{-1}g_{7/2}$ configuration reproduce reasonably well the experimental ratios in Fig. 8(a). In the calculation, $Q_0=3.0$ *e* b was assumed. In ^{119}I the comparison of experimental and theoretical $B(M1)/B(E2)$ ratios for the $g_{9/2}^{-1}$ band gives an estimate of $Q_0\approx 3.1$ *e* b [26] and a similar analysis in ^{117}Sb for the same band using the branching ratios of Ref. [14] yields $Q_0\approx 2.7$ *e* b. Thus, the quadrupole moment used for the $g_{9/2}^{-1}g_{7/2}$ configuration in ^{118}Te is consistent with those for the $g_{9/2}^{-1}$ bands in the $Z-1$ and $Z+1$ isotones.

Due to the close proximity of the proton $d_{5/2}$ and $g_{7/2}$ states, another strongly coupled band close in energy to band 6 is expected. The 3079 and 3168 keV states with feeding 300 and 261 keV transitions, respectively, are candidates for the band head of such a band.

The parity of band 7 was not determined in the present work. Based on observations in the neighboring ^{117}Sb, ^{119}I, and ^{120}Xe nuclei [14,26,29], three different configurations can be considered for this band. The proton $g_{9/2}^{-1}h_{11/2}$ configuration can be ruled out because the *K* value extracted for band 7 is too large compared with the expected $K=5$. Furthermore, the $B(M1)/B(E2)$ ratios in band 7 are quite different to those in the $g_{9/2}^{-1}h_{11/2}$ band in ^{120}Xe [29]. Another possibility is that this band is built on the $\pi g_{9/2}^{-1}g_{7/2}\nu h_{11/2}^2$ configuration, but then it would be somewhat strange that there is no decay to band 6. Finally, if band 7 is of positive parity, it may be built upon the $\pi g_{9/2}^{-1}g_{7/2}\nu h_{11/2}g_{7/2}$ configuration (where the last neutron could be replaced by the $d_{5/2}$ or $d_{3/2}$). The band head energy of such a band can be roughly estimated from the energy of the $\pi g_{9/2}^{-1}\nu h_{11/2}g_{7/2}$ band head in ^{117}Sb and ^{119}I [14,26] to be about 5 MeV. This is in excellent agreement with the band head energy of band 7. As can be seen from Fig. 8(b), the experimental $B(M1)/B(E2)$ ratios are nicely reproduced in the model calculations assuming such a configuration.

D. Intruder states

Excited 0^+ states with associated rotational bands are well established in Sn nuclei. These states are built on proton $2p$-$2h$ excitation across the $Z=50$ shell gap. In Cd nuclei having two protons less, the lowest excited 0^+ state in $^{106-114}$Cd and the second excited 0^+ state in $^{116-122}$Cd have been identified as intruder states [34]. These states are strongly populated in two-proton transfer reactions [35] and they form a V-shaped pattern centered at $N=66$, as the $2p$-$2h$ intruder states in Sn nuclei. Bands built on these intruder 0^+ states have also been found in Cd nuclei. In Cd nuclei, however, the situation with the intruder states is more ambiguous than in Sn nuclei. As pointed out in Ref. [34], the suggested 0^+ band head of the intruder band plays in the vibrator picture the role of the two-quadrupole phonon state with an enhanced $E2$ transition to the yrast 2^+ state. Furthermore, the role of mixing between the intruder and vibrational states and the role of the $h_{11/2}$ neutrons in the lighter isotopes are still intriguing questions.

Previously, the best evidence for the existence of the low-lying intruder states built on the proton $2p$-$2h$ excitations in Te nuclei was the systematics of the first excited 0^+ states [4]. They display a V-shaped pattern centered at $N=66$, in

accordance with the 0^+ intruder states in Cd and Sn nuclei. As in the Cd nuclei, the $E2$ transition from the possible intruder 0^+ state at 958 keV to the yrast 2^+ state is fast in ^{118}Te, indicating that this state is a two-phonon state in the vibrator picture.

The observation of several deformed bands in ^{118}Te gives new arguments for the discussion of zero-quasiparticle intruder states. One can compare the excitation energies of the deformed bands involving proton $2p$-$2h$ excitations in ^{118}Te relative to the supposed deformed 0^+ state at 958 keV with those in neighboring nuclei. In ^{120}Xe the proton 9^- states lie at 3151 ($\pi g_{9/2}h_{11/2}$) and 2972 keV ($\pi g_{7/2}h_{11/2}$) [29]. The corresponding states are not known in ^{116}Sn, but in ^{114}Sn the 9^- state of the proton $h_{11/2}g_{9/2}$ band lies at 2970 keV above the intruder 0^+ state (at 1954 keV) [36]. In ^{118}Te the 9^- state of the $\pi g_{7/2}h_{11/2}$ band is 2722 keV above the 958 keV 0^+ state. The assumption of the intruder character of the 958 keV 0^+ state is therefore quite reasonable.

In the calculated potential energy surface there is no minimum at a well deformed prolate shape for low spin values. However, there is a shoulder present in the potential energy surface at $\epsilon_2 = 0.20$–0.25 and $\gamma \approx 0°$ [see Fig. 5(a)], close to the nuclear shape expected for the intruder band in Sn nuclei. At higher spins, due to its large moment of inertia, the prolate-deformed configuration is expected to become energetically more favored.

Possible candidates for the positive parity proton $4p$-$2h$ intruder states in ^{118}Te are displayed in Fig. 9. As discussed earlier, the level spacings in the intruder band in ^{118}Te should resemble those in the proton $2p$-$4h$ band in ^{114}Cd. However, this band is only known up to $I = 6\hbar$ [5]. Instead, ground-state bands of ^{110}Ru and ^{122}Ba [37,38] are shown in Fig. 9. In the simple intruder-spin picture [39], level spacings in these proton $6h$ and $6p$ bands should also be similar to those in the $4p$-$2h$ band in ^{118}Te. Also shown is the intruder band in ^{116}Sn. In this band the 0^+ and 4^+ states are mixed with the first excited 0^+ state and the yrast 4^+ state, respectively [25]. This demonstrates how the mixing of states may perturb the level pattern in the intruder band. As discussed earlier, the available states in ^{118}Te do not form any regular band below $I = 6$. However, at higher spins in Fig. 9 there are two $E2$ sequences, which resemble the expected level pattern of the $4p$-$2h$ intruder band. If the 3000 keV 8^+, 3835 keV 10^+, and 4746 keV 12^+ states being connected by $E2$ transitions, are assigned to the intruder band, the band head should lie close to first excited 0^+ state. On the other hand, if band 1 is interpreted as the intruder band, the unperturbed band head might lie somewhere between the first and second (at 1517 keV) excited 0^+ states. It remains to be seen in future experiments, whether either one of these $E2$ sequences is related to the zero-quasiparticle intruder states.

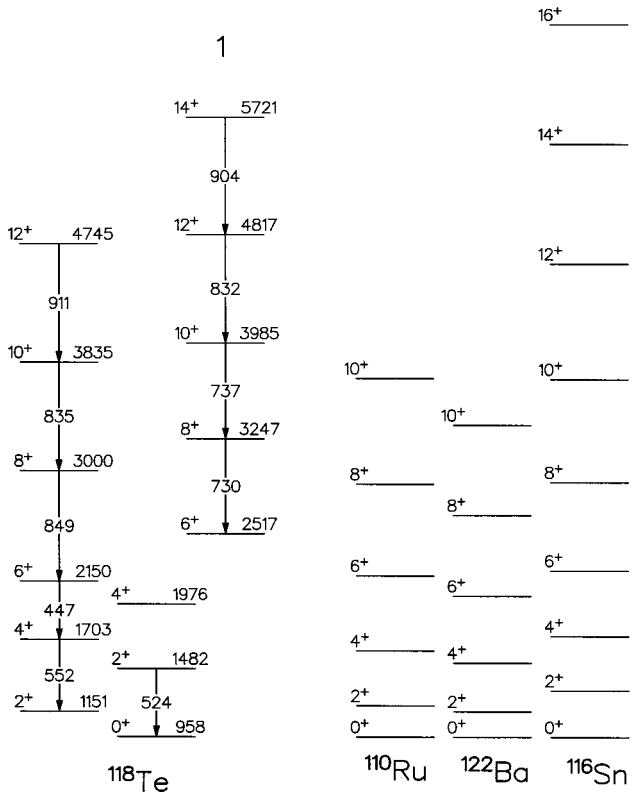

FIG. 9. Candidates for proton $4p$-$2h$ states in ^{118}Te together with the ground-state bands in the $6h$ ^{110}Ru and $6p$ ^{122}Ba nuclei [37,38]. Also shown is the intruder band in ^{116}Sn built on proton $2p$-$2h$ excitations [25].

E. Noncollective states

Level structures labeled $Y1$, $Y2$, $N1$, and $N2$ are irregular and most likely involve noncollective states. Such level structures have also been observed in the neighboring even-mass Te nuclei [19,17,40]. Theoretical calculations based on the TRS approach predict noncollective oblate ($\gamma = +60°$) states to be yrast at certain spin values [28]. These calculations suggest that in ^{118}Te the 14^-, 16^+, 19^-, and 22^- states built on fully aligned $\pi g_{7/2}^2 \nu d_{5/2} h_{11/2}$, $\pi g_{7/2}^2 \nu h_{11/2}^2$, $\pi g_{7/2} h_{11/2} \nu h_{11/2}^2$, and $\pi g_{7/2}^2 \nu d_{5/2} h_{11/2}^3$ configurations, respectively, are particularly favored. Based on the theoretical predictions, the 5238 keV 14^-, 5347 keV 16^+, $(6759+\Delta)$ keV 19^-, and $(8234+\Delta)$ keV 22^- states have previously been associated with those configurations [19,28]. The observed 1.4(2) ns mean lifetime can most readily be attributed to the $(6759+\Delta)$ keV level decaying by very low energy transitions to states of different origin.

In the following, the level structures $Y1$, $Y2$, $N1$, and $N2$ are interpreted in terms of number of $h_{11/2}$ protons and neutrons. The states in groups $N1$ and $N2$ involve neutron $g_{7/2}h_{11/2}^n$ and $d_{5/2}h_{11/2}^n$ configurations with an odd number of $h_{11/2}$ neutrons. In the sequence $Y2$ the 6^+ and 10^+ states have been associated with the proton $g_{7/2}^2$ and neutron $h_{11/2}^2$ configurations, respectively [19]. The higher lying states involve the proton $g_{7/2}^2$ configuration and/or an even number of $h_{11/2}$ neutrons. Similarly to groups $N1$ and $N2$, group $Y2$ does not involve protons excited to the $h_{11/2}$ state.

Provided that the lowest states in band $Y1$ are of negative parity, the $I = 19$ and 22 states can be associated with the oblate configurations suggested in Refs. [19,28]. The configuration $\pi g_{7/2}^2 \nu g_{7/2} h_{11/2}^3$ yields a state with spin and parity of 23^-, possibly corresponding either one of the $I = (23)$ states close to 9 MeV excitation energy. States with higher

angular momentum in band $Y1$ may arise from the $\pi g_{7/2}h_{11/2}\nu h^3_{11/2}$ configuration coupled to the $d_{5/2}$ or $g_{7/2}$ neutrons, which gives positive parity states with $I_{max}=25$ and 26, respectively. Therefore, the configuration of most states in band $Y1$ contains a proton on the $h_{11/2}$ orbital.

IV. SUMMARY

The γ decay of excited states in ^{118}Te have been investigated following (Hi,xn) reactions. Eight rotational bands were identified. Three of the bands were constructed up to the I$\approx 30\hbar$ region. They were interpreted as based upon configurations involving one or two protons on the deformation driving $h_{11/2}$ orbital coupled to proton $2p$-$2h$ excitations of the core. The neutron $h^2_{11/2}$ alignment appears to be smoothed out in these bands, as in related bands in the isotones of ^{118}Te. The existence of $4p$-$2h$ intruder states at low spin have been discussed and candidates for intruder band members presented. Bands characterized by intense dipole transitions were associated with configurations having a hole on the proton $g_{9/2}$ orbital.

ACKNOWLEDGMENTS

We are grateful to the staff at JYFL for providing excellent beam and technical support. We express sincere thanks to Y.R. Shimizu for providing the PES calculation. This work was supported by the Academy of Finland and the access to Large Scale Facility program of the European Union.

[1] J. Bron, W. H. A. Hesselink, A. van Poelgeest, J. J. A. Zalmstra, H. J. Uitzinger, H. Verheul, K. Heyde, M. Varoquier, H. Vincx, and P. van Isacker, Nucl. Phys. **A318**, 335 (1979).

[2] A. K. Gaigalas, R. E. Shroy, G. Schatz, and D. B. Fossan, Phys. Rev. Lett. **35**, 555 (1975); Phys. Rev. C **19**, 1324 (1979).

[3] J. L. Wood, K. Heyde, W. Nazarewicz, M. Huyse, and P. van Duppen, Phys. Rep. **215**, 101 (1992).

[4] R. Julin, Phys. Scr. **T56**, 151 (1995).

[5] S. Juutinen, R. Julin, P. Jones, A. Lampinen, G. Lhersonneau, E. Mäkelä, M. Piiparinen, A. Savelius, and S. Törmänen, Phys. Lett. B **386**, 80 (1996).

[6] R. Wadsworth, H. R. Andrews, R. M. Clark, D. B. Fossan, A. Galindo-Uribarri, J. R. Hughes, V. P. Janzen, D. R. LaFosse, S. M. Mullins, E. S. Paul, D. C. Radford, H. Schnare, P. Vaska, D. Ward, J. N. Wilson, and R. Wyss, Nucl. Phys. **A559**, 461 (1993).

[7] R. Wadsworth, C. W. Beausang, M. Gromaz, J. DeGraaf, T. E. Drake, D. B. Fossan, S. Flibotte, A. Galindo-Uribarri, K. Hauschild, I. M. Hibbert, G. Hackman, J. R. Hughes, V. P. Janzen, D. R. LaFosse, S. M. Mullins, E. S. Paul, D. C. Radford, H. Schnare, P. Vaska, D. Ward, J. N. Wilson, and I. Ragnarsson, Phys. Rev. C **53**, 2763 (1996).

[8] V. P. Janzen, D. R. LaFosse, H. Schnare, D. B. Fossan, A. Galindo-Uribarri, J. R. Hughes, S. M. Mullins, E. S. Paul, L. Persson, S. Pilotte, D. C. Radford, I. Ragnarsson, P. Vaska, J. C. Waddington, R. Wadsworth, D. Ward, J. Wilson, and R. Wyss, Phys. Rev. Lett. **72**, 1160 (1994).

[9] D. R. LaFosse, D. B. Fossan, J. R. Hughes, Y. Liang, H. Schnare, P. Vaska, M. P. Waring, J.-y. Zhang, R. M. Clark, R. Wadsworth, S. A. Forbes, E. S. Paul, V. P. Janzen, A. Galindo-Uribarri, D. C. Radford, D. Ward, S. M. Mullins, D. Prévost, and G. Zwartz, Phys. Rev. C **50**, 1819 (1994).

[10] V. P. Janzen, H. R. Andrews, B. Haas, D. C. Radford, D. Ward, A. Omar, D. Prévost, M. Sawicki, P. Unrau, J. C. Waddington, T. E. Drake, A. Galindo-Uribarri, and R. Wyss, Phys. Rev. Lett. **70**, 1065 (1993).

[11] E. S. Paul, V. P. Janzen, D. C. Radford, D. Ward, S. M. Mullins, D. B. Fossan, D. R. LaFosse, H. Schnare, H. Timmers, P. Vaska, R. M. Clark, and R. Wadsworth, Phys. Rev. C **50**, 2297 (1994).

[12] R. S. Chakrawarthy and R. G. Pillay, Phys. Rev. C **54**, 2319 (1996).

[13] D. R. LaFosse, D. B. Fossan, J. R. Hughes, Y. Liang, P. Vaska, M. P. Waring, and J.-y. Zhang, Phys. Rev. Lett. **69**, 1332 (1992).

[14] D. R. LaFosse, D. B. Fossan, J. R. Hughes, Y. Liang, H. Schnare, P. Vaska, M. P. Waring, and J.-y. Zhang, Phys. Rev. C **56**, 760 (1997).

[15] E. S. Paul, C. W. Beausang, S. A. Forbes, S. J. Gale, A. N. James, P. M. Jones, M. J. Joyce, H. R. Andrews, V. P. Janzen, D. C. Radford, D. Ward, R. M. Clark, K. Hauschild, I. M. Hibbert, R. Wadsworth, R. A. Cunningham, J. Simpson, T. Davinson, R. D. Page, P. J. Sellin, P. J. Woods, D. B. Fossan, D. R. LaFosse, H. Schnare, M. P. Waring, A. Gizon, J. Gizon, T. E. Drake, J. DeGraaf, and S. Pilotte, Phys. Rev. C **50**, 698 (1994).

[16] I. Thorslund, D. B. Fossan, D. R. LaFosse, H. Schnare, K. Hauschild, I. M. Hibbert, S. M. Mullins, E. S. Paul, I. Ragnarsson, J. M. Sears, P. Vaska, and R. Wadsworth, Phys. Rev. C **52**, R2839 (1995).

[17] J. M. Sears, D. B. Fossan, I. Thorslund, P. Vaska, E. S. Paul, K. Hauschild, I. M. Hibbert, R. Wadsworth, S. M. Mullins, A. V. Afanasjev, and I. Ragnarsson, Phys. Rev. C **55**, 2290 (1997).

[18] J. J. van Ruyven, W. H. A. Hesselink, J. Akkermans, P. van Nes, and H. Verheul, Nucl. Phys. **A380**, 125 (1982).

[19] A. Sharma, J. Singh, H. Kaur, J. Goswamy, D. Mehta, N. Singh, P. N. Trehan, E. S. Paul, and R. K. Bhowmik, Z. Phys. A **351**, 131 (1996).

[20] P. J. Nolan, D. W. Gifford, and P. J. Twin, Nucl. Instrum. Methods Phys. Res. A **236**, 95 (1985).

[21] D. C. Radford, Nucl. Instrum. Methods Phys. Res. A **361**, 297 (1995).

[22] S. Juutinen, R. Julin, M. Piiparinen, P. Ahonen, B. Cederwall, C. Fahlander, A. Lampinen, T. Lönnroth, A. Maj, S. Mitarai, D. Müller, J. Nyberg, P. Ŝimeĉek, M. Sugawara, I. Thorslund, S. Törmänen, A. Virtanen, and R. Wyss, Nucl. Phys. **A573**, 306 (1994).

[23] *Table of Isotopes*, 8th ed., edited by R. B. Firestone, V. S.

Shirley, C. M. Baglin, S. Y. F. Chu, and J. Zipkin (Wiley, New York, 1996).

[24] R. Bengtson and S. Frauendorf, Nucl. Phys. **A314**, 27 (1979); **A327**, 139 (1979).

[25] A. Savelius, S. Juutinen, K. Helariutta, P. Jones, R. Julin, P. Jämsen, M. Muikku, M. Piiparinen, J. Suhonen, S. Törmänen, R. Wyss, P. T. Greenlees, P. Simecek, and D. Cutoiu, Nucl. Phys. **A637**, 491 (1998).

[26] S. Törmänen, S. Juutinen, R. Julin, A. Lampinen, E. Mäkelä, M. Piiparinen, A. Savelius, A. Virtanen, G. B. Hagemann, Ch. Droste, W. Karczmarczyk, T. Morek, J. Srebrny, and K. Starosta, Nucl. Phys. **A613**, 282 (1997).

[27] Y. R. Shimizu, E. Vigezzi, and R. A. Broglia, Nucl. Phys. **A509**, 80 (1990).

[28] E. S. Paul, D. B. Fossan, J. M. Sears, and I. Thorslund, Phys. Rev. C **52**, 2984 (1995).

[29] S. Törmänen, S. Juutinen, R. Julin, B. Cederwall, A. Johnson, R. Wyss, P. Ahonen, B. Fant, M. Matsuzaki, J. Nyberg, M. Piiparinen, S. Mitarai, J. Mukai, and A. Virtanen, Nucl. Phys. **A572**, 417 (1994).

[30] A. D. Efimov and Yu. N. Lobach, Yad. Fiz. **61**, 401 (1998) [Phys. At. Nucl. **61**, 341 (1998)].

[31] F. Dönau and S. Frauendorf, *Proceedings of the Conference on High Angular Momentum Properties of Nuclei*, Oak Ridge, 1982, edited by N. R. Johnson (Harwood, New York, 1983), p. 143; F. Dönau, Nucl. Phys. **A471**, 469 (1987).

[32] D. C. Radford, H. R. Andrews, G. C. Ball, D. Horn, D. Ward, F. Banville, S. Flipotte, S. Monaro, S. Pilotte, P. Taras, J. K. Johansson, D. Tucker, J. C. Waddington, M. A. Riley, G. B. Hagemann, and I. Hamamoto, Nucl. Phys. **A545**, 665 (1992).

[33] T. Lönnroth, S. Vajda, O. C. Kistner, and M. H. Rafailovich, Z. Phys. A **317**, 215 (1984).

[34] J. Kumpulainen, R. Julin, J. Kantele, A. Passoja, W. H. Trzaska, E. Verho, J. Väärämäki, D. Cutoiu, and M. Ivascu, Phys. Rev. C **45**, 640 (1992).

[35] H. W. Fielding, R. E. Anderson, C. D. Zafiratos, D. A. Lind, F. E. Cecil, H. H. Wieman, and W. P. Alford, Nucl. Phys. **A281**, 389 (1977).

[36] M. Schimmer, R. Wirowski, S. Albers, G. Böhm, A. Dewald, A. Gelberg, and P. von Brentano, Z. Phys. A **338**, 117 (1991).

[37] J. L. Durell (unpublished).

[38] R. Wyss, A. Johnson, F. Liden, J. Nyberg, A. H. Nelson, D. W. Banes, A. Kirwan, D. J. G. Love, and J. Simpson (unpublished).

[39] K. Heyde, J. Jolie, J. Moreau, J. Ryckebush, M. Waroquier, P. van Duppen, M. Huyse, and J. L. Wood, Nucl. Phys. **A466**, 189 (1987).

[40] E. S. Paul, D. B. Fossan, G. J. Lane, J. M. Sears, I. Thorslund, and P. Vaska, Phys. Rev. C **53**, 1562 (1996).